ACS Catalysis

Research Article

pubs.acs.org/acscatalysis

Structure and Activity of Photochemically Deposited "CoPi" Oxygen Evolving Catalyst on Titania

Rony S. Khnayzer,[†] Michael W. Mara,[‡,§] Jier Huang,[‡,§] Megan L. Shelby,[‡,§] Lin X. Chen,*[,‡,§] and Felix N. Castellano*[,†]

[†]Department of Chemistry and Center for Photochemical Sciences, Bowling Green State University, Bowling Green, Ohio 43403, United States

[‡]Chemical Sciences and Engineering Division, Argonne National Laboratory, Argonne, Illinois 60439, United States

[§]Department of Chemistry, Northwestern University, Evanston, Illinois 60208-3113, United States

Supporting Information

ABSTRACT: The cobalt phosphate "CoPi" oxygen evolving catalyst (OEC) was photochemically grown on the surface of TiO_2 photoanodes short-circuited to a Pt wire under bandgap illumination in the presence of $Co(NO_3)_2$ and sodium phosphate (NaPi) buffer. Extended photodeposition (15 h) using a hand-held UV lamp readily permitted quantitative structural and electrochemical characterization of the photochemically deposited CoPi OEC on titania. The formed catalytic material was characterized by scanning electron microscopy (SEM) and energy dispersive X-ray (EDX) spectroscopy experiments, illustrating the production of easily visualized micrometer scale clusters throughout the titania surface containing both cobalt and phosphate. X-ray absorption fine structure (XAFS) and X-ray absorption near edge structure (XANES) studies indicated that the newly formed material was structurally consistent with the production of molecular cobaltate clusters composed of a cobalt oxide core that is most likely terminated by phosphate ions. The oxidation state, structure, and the oxygen evolution activity of this CoPi catalyst photochemically grown on titania were quantitatively similar to the analogous electrodeposited materials on titania as well as those produced on other electroactive substrates. From pH-dependent electrochemical measurements, proton-coupled electron transfer was shown to be an important step in the oxygen evolution mechanism from the photodeposited OEC clusters on TiO_2 in agreement with previous reports on other materials. Similarly, the utilization of $NaClO_4$ as electrolyte during the controlled potential electrolysis experiments failed to maintain an appreciable current density, indicating that the catalyst was rendered inactive with respect to the one immersed in NaPi. The requirement of having phosphate present for long-term catalytic activity implied that the same "repair" mechanism might be invoked for the hybrid materials investigated here. The OEC catalyst operated at Faradaic efficiencies close to 100% in controlled potential electrolysis experiments, indicating that the holes relayed to the photodeposited CoPi are indeed selective for promoting water oxidation on titania.

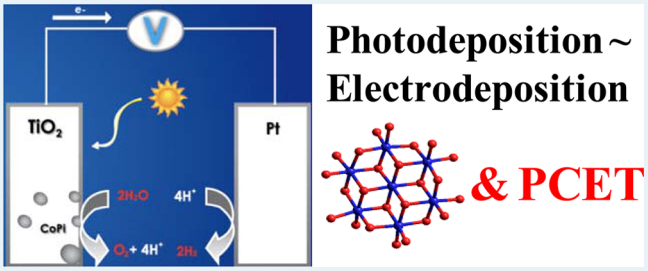

KEYWORDS: *cobalt phosphate, CoPi, titania, structure, water oxidation, oxygen evolution, photodeposition*

INTRODUCTION

Generating chemical fuels from the energy of photons supplied by the sun is a challenging problem requiring the development of complex catalytic systems desirably from earth abundant materials.[1−5] The earth's population is expected to markedly increase over the following century and is forecast to lead to historically unprecedented energy consumption.[6,7] If the human race continues burning fossil fuels to meet these increasing energy demands, the unparalleled CO_2 release into the atmosphere represents a serious threat that may forever modify the terrestrial climate.[6,8] Fortunately, the energy supplied by the sun far exceeds that of future consumption demands and harvesting only a fraction of this energy could significantly decrease our reliance on fossil fuels.[9,10] As the sun is diurnal, systems capable of storing solar energy for later use are required. Rechargeable batteries have been used in this regard in tandem with photovolatic (PV) solar panels but suffer from high cost, low discharge capacity, and short operational lifetimes when compared to the conjoined PV materials. Alternatively, light energy stored in the form of chemical bonds represents a viable strategy for combining PVs with appropriate reactions to generate desirable high-energy products.[11,12] One such reaction is water splitting, which is a thermodynamically uphill process (eqs 1−3), and light energy would be stored via photodriven electrolysis in hydrogen and oxygen bonds, desirable feedstock chemicals for fuel cells.[6,9,10,13,14] Addition-

Received: August 2, 2012
Revised: September 7, 2012
Published: September 10, 2012

ally, the exothermic combustion of H_2 (the reverse of eq 3) provides a potential carbon-free energy source that yields water as product.

$$O_2 + 4H^+ + 4e^- \rightarrow 2H_2O \quad E_{anodic} = 1.23 - 0.059(pH) \quad (1)$$

$$4H^+ + 4e^- \rightarrow 2H_2 \quad E_{cathodic} = 0 - 0.059(pH) \quad (2)$$

$$--- \quad [V \text{ vs NHE}]$$

$$2H_2O \rightarrow 2H_2 + O_2 \quad E_{reaction} = -1.23\ V \quad (3)$$

Modern advances in electrocatalysis appear promising toward the development of earth abundant materials that can effectively promote each necessary half-reaction (eqs 1 and 2) ultimately resulting in water splitting.[15−19] Arguably, oxidation is the more difficult step in the water splitting reaction that requires a merging of four hole equivalents and two oxygen atoms, eq 1.[18,20−22] More than 30 years ago, Shafirovich and co-workers originally used cobalt ions in the presence of buffered aqueous solutions resulting in the production of oxygen catalytically from water.[23,24] However the material produced was ill characterized and the mechanism for water oxidation was not rationalized. Recently, Nocera and co-workers have developed and extensively characterized a water oxidation electrocatalyst composed of cobalt and inorganic phosphate, termed CoPi, which operates in neutral water at low overpotentials (η < 400 mV) and features a regenerative self-healing mechanism following catalyst dissolution.[11,17,25,26] The oxygen production mechanism of this electrochemically grown catalyst was suggested to be very similar to the S-state pumping of photosystem II in plants also known as the Kok cycle where the manganese metal centers undergo a series of oxidation/reduction reactions concomitant with proton and electron transfer processes.[11,17,25−29] The structure, valency, and oxygen evolution mechanism of the electrochemically active cobalt species have been assigned to a Co oxo/hydroxo species whose oxidation numbers vary between 2, 3, and 4 in a series of proton and electron transfer reactions prior to the oxygen evolution step.[26,28−34]As the photogenerated holes of many semiconductors can provide potentials adequate to drive CoPi catalyst formation, Choi and co-workers recently demonstrated such a photochemical route successfully applied to a variety of *n*-type semiconductors.[35−37] In such hybrid materials, upon Co(II) oxidation to Co(III) using a photogenerated hole at the surface, an oxide is produced and immediately precipitates on the surface of the semiconductor owing to its low solubility in buffered aqueous solutions.[37] To date, this catalyst has been grown using three different methodologies, namely, electrochemical, photochemical, and photoassisted electrochemical on the surfaces of various electrodes[27] as well as different semiconductors including ZnO,[37] Fe_2O_3,[36,38−41] WO_3,[42] $BiVO_4$,[43−45] TaON,[46] and Si.[12,47,48] The advantage of photodepositing CoPi on semiconductors is that the density of the catalyst formed would presumably be large where the holes are highly accessible to operating the desired water oxidation chemistry.[37,47] To photochemically deposit CoPi, two different routes can potentially be applied, short-circuit and open circuit deposition. In short-circuit photodeposition, the semiconductor is submerged in phosphate buffer containing the Co(II) precursor, and the photogenerated holes in the valence band are used to oxidize cobalt ions. The Co(III) species can then deposit as an oxide on the surface of the photoactive material. While this method can lead to the photodeposition of cobalt oxide, unfortunately, the reduction of Co(III) to Co(II) by electrons trapped in the conduction band is also thermodynamically favorable. To decrease the likelihood of the catalyst reverting back to the starting Co(II) material, electrons are simply short-circuited to a platinum electrode placed remotely from the titania to prevent this undesirable chemistry. For example, the short-circuit method has yielded superior CoPi water oxidation catalysts in comparison to those produced using the analogous open-circuit procedure (conduction band electrons are trapped in the same vicinity as the oxidized Co(III) species) in Fe_2O_3.[36] These results were mainly attributed to the increase of the catalyst's nucleation density and a corresponding increase in the "average" oxidation number of the resting CoPi catalyst.[36]

To the best of our knowledge, no structural characterization of the photodeposited CoPi OEC on metal oxide semiconductors has been provided in the literature. In the present study, we were interested in determining the structure and activity of this photogenerated catalyst deposited on the surface of titania electrodes, which is essential for the development of stand-alone systems capable of growing the catalyst and sustaining long-term water oxidation chemistry at a biased electrode. Titania or TiO_2 is characterized by high stability in aqueous solutions under a wide pH range and possesses a very positive valence band potential poised >1 eV overpotential to facilitate both CoPi deposition and water oxidation.[49−51] We therefore selected the TiO_2 support to characterize the CoPi catalyst formed on the surface without complications associated with semiconductor corrosion processes. Despite its wide bandgap of 3.0−3.2 eV, rendering absorption only in the UV portion of the spectrum, TiO_2 was used by Fujishima and Honda in the first photoelectrochemical water splitting device reported using solar illumination. In these early studies,[52] TiO_2 was operated under extreme pH values and was not interfaced with any catalyst. However, the presence of appropriate catalysts on the surface can increase the quantum yield of water splitting by avoiding unwanted oxidation reactions thereby rendering this facile photochemistry feasible under benign conditions by decreasing the barrier for water oxidation.[42] For example, a simple cobalt treatment markedly enhanced the visible light photoelectrochemical properties of N-modified TiO_2 nanowires in basic solution through passivation of surface states, subsequently facilitating water oxidation chemistry.[53] Similar observations were previously described on α-Fe_2O_3 films treated with Co(II) ions.[54] In this study we report the photochemical growth of the CoPi catalyst on the surface of electroactive TiO_2 films prepared by the sol−gel method on conducting fluorine-doped tin oxide (FTO) glass substrates. Scanning electron microscopy (SEM) and energy dispersive X-ray (EDX) spectroscopy characterized the bulk properties of the photogenerated catalyst with ultimate structural determination by X-ray absorption fine structure (XAFS) spectroscopy taken in a quasi in situ state. The electrochemical and photoelectrochemical properties of the new material were quantitatively compared to the previously reported electrochemically deposited CoPi catalyst.

EXPERIMENTAL SECTION

General Procedures. Cobalt nitrate hexahydrate, titanium isopropoxide, hydroxypropyl cellulose (M_n = 10 000, M_w = 80 000), cobalt oxide (CoO), and glacial acetic acid were purchased from Aldrich. Cobaltic oxide (Co_2O_3) was obtained as a black powder from J.T. Baker. Sodium hydrogen phosphate heptahydrate and sodium dihydrogen phosphate dihydrate

dx.doi.org/10.1021/cs3005192 | ACS Catal. 2012, 2, 2150−2160

were purchased from Alfa Aesar and used as received. Fluorine-doped tin oxide (FTO) conducting glass substrates (TEC 15) were purchased from Hartford Glass. Water was deionized using a Barnstead nanopure system. All reagent grade solvents and reactants were used as received. Thickness of the TiO_2 films was measured by a KLA-Tencor Alpha-Step IQ Surface Profiler. Electrochemical measurements were performed using a Bioanalytical Systems Epsilon electrochemical workstation in a three-electrode arrangement. The SEM images were acquired on a Hitachi S-2700 equipped with an EDX genesis energy dispersive X-ray spectroscopy detector at 10−20 keV acceleration voltage. The photodeposition of CoPi was achieved by using a 4 W compact UV hand-held lamp at λ_{ex} = 365 nm. The light source in the photoelectrochemical experiments was a 300 W xenon arc lamp (Oriel) whose output was passed through a water filter. The 200 mW/cm^2 broadband illumination was realized by coupling a bifurcated fiber bundle to the experiment. The oxygen produced was measured using a gas chromatograph (Shimadzu GC-8A, argon carrier gas) equipped with a 5 Å molecular sieve column (Restek) and thermal conductivity detector.

Colloidal TiO_2 Synthesis. The TiO_2 paste was prepared according to a literature procedure.[55,56] Briefly, a solution containing titanium(IV) isopropoxide (37 mL) and isopropanol (10 mL) was added dropwise to a mixture of glacial acetic acid (80 mL) and water (250 mL) at ∼0 °C as measured by a thermometer immersed in the solution. This temperature can be maintained by submersing the flask in an acetone bath and occasionally adding dry ice. The resulting solution changes from colorless to white when heated to 80 °C, and finally maintained at this temperature for an additional 8 h with stirring. After cooling to room temperature, 80 mL of the resultant solution was sonicated for 5 min using a high energy sonicator (Branson Sonifier 250), and finally maintained at 230 °C over 8 h while stirring in a titanium autoclave (Parr Instrument Company). The final TiO_2 colloidal solution at room temperature was sonicated for 5 min and concentrated to 12 wt % (TiO_2) using a rotary evaporator (30 °C, 30 Torr). Hydroxypropyl cellulose (6 wt %) previously dissolved in water was added slowly to the final mixture, and the paste produced was maintained under constant stirring until used to prepare the titania electrodes.

TiO_2 Film Formation on Conductive Glass. FTO conducting glass substrates were cleaned using conventional sonication, first with a solution of HCl in isopropanol, then a solution of soap in water, then finally acetone. The FTO glass was then dried in an oven. TiO_2 (12 wt %) and hydroxypropylcellulose (6 wt %) in water:glacial acetic acid (3:1 by volume) was sonicated and stirred vigorously overnight. The resultant paste was doctor bladed on FTO glass between 3 Scotch tape layers resulting in a TiO_2 electrode area of ∼1 cm^2 and ∼8 μm thickness. The electrode was sintered at 500 °C for 30 min at a heating rate of 5 °C per min and finally cooled to room temperature.

O_2 Evolution Measurements. Oxygen evolution during electrochemical and photoelectrochemical measurements was detected from the headspace of an airtight H-cell of known headspace volume. The H-cell contained two compartments separated by a frit of medium porosity, the working compartment contained the working electrode and the reference electrode (Ag/AgCl), and the auxiliary compartment contained the counter electrode (Pt wire). The solution and headspace were deaerated by continuous argon bubbling for 1 h prior to the experiment. At all times the solutions were stirred at constant rate using a stir bar when the electrochemical and photoelectrochemical controlled potential electrolysis were acquired. Gas samples were withdrawn from the working compartment using a 100 μL gastight syringe (Hamilton), whose contents were injected and analyzed in a gas chromatograph (Shimadzu GC-8A, argon carrier gas) equipped with a 5 Å molecular sieve column (Restek) and thermal conductivity detector. O_2 produced was calculated by extrapolation from a calibration curve. The GC yielded a constant ratio for O_2:N_2 area in all samples of ambient air. Therefore, the O_2 contribution from residual air was simply subtracted from the measured O_2 area to obtain the actual O_2 evolved from the analyzed reaction. Oxygen evolved was corrected using Henry's law to account for the amount of dissolved oxygen in the electrolyte solutions.

Photodeposition, Electrodeposition, and Photoelectrochemistry. In all the photodeposition, electrochemical, and photoelectrochemical experiments presented herein, the ohmic contact to the TiO_2 electrode was achieved by using copper tape between the FTO support and a thick Ag wire that was attached to external alligator clips. The connections were then wrapped with Kapton nonconductive tape to provide mechanical support and electrical insulation. In a fused silica photoelectrochemical cell equipped with home-built Teflon cap that snuggly fits all the electrodes, the photodeposition of CoPi was achieved by front-side bandgap illumination of the TiO_2 films immersed in a solution of 0.5 mM $Co(NO_3)_2$ in 0.1 M of sodium phosphate (NaPi) buffer at pH 7, using a hand-held UV lamp (λ_{ex} = 365 nm) over the course of 15 h. During the photodeposition, the films were short-circuited to a platinum wire using an external copper conducting wire equipped with alligator clips.[36] In control experiments, Co^{2+} ions were simply adsorbed onto the TiO_2 electrodes under the same conditions with the excitation light off. The electrodeposited catalyst studied by XAFS was grown by applying a 1.1 V (vs Ag/AgCl) bias to the TiO_2 electrode immersed in a solution of 0.5 mM $Co(NO_3)_2$ in 0.1 M of NaPi buffer at pH 7. The electrodeposition was allowed to proceed for two hours under a current density of ∼0.5 mA/cm^2. The electrochemical and photoelectrochemical characterization of the resultant films were performed using a three electrode arrangement where the TiO_2/CoPi material was used as a working electrode, Ag/AgCl as a reference electrode, and a Pt wire as auxiliary electrode in an airtight H-cell equipped with stir bars. The 200 mW/cm^2 fiber optic output of the xenon lamp was used for backside illumination (through the FTO support) to measure the resultant photocurrents. All electrochemical and photoelectrochemical measurements were accomplished without *iR* compensation except for the Tafel plots presented in Figure 7. In all electrochemical experiments presented, potentials were measured against Ag/AgCl, where $V_{NHE} = V_{Ag/AgCl} + 0.197$ V.

XAFS and XANES Measurements of CoPi on Titania. The cobalt K-edge X-ray absorption near edge structure (XANES) and X-ray absorption fine structure (XAFS) spectra were collected at beamline 12BM at the Advanced Photon Source of Argonne National Laboratory. Si(111) double crystals were used in the monochromator. The X-ray absorption spectra at the cobalt K-edge of the CoPi/TiO_2 films (electrochemically and photochemically deposited CoPi on TiO_2, along with the control sample where Co(II) salt solution was simply adsorbed onto the TiO_2 electrode) were collected by the fluorescence detection mode, using a Canberra

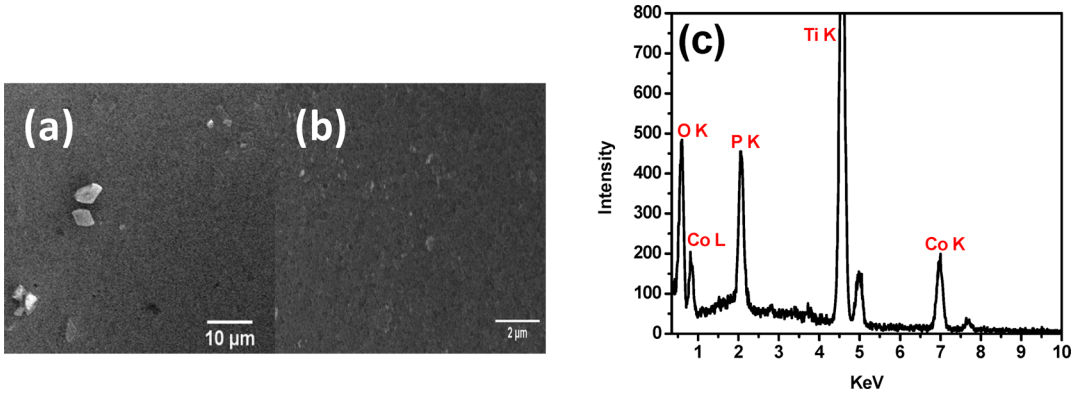

Figure 1. (a, b) SEM images of the CoPi catalyst after 15 h photodeposition on TiO_2 substrate. (c) EDX spectrum of the catalyst. The elemental analysis shows the presence of cobalt and phosphate.

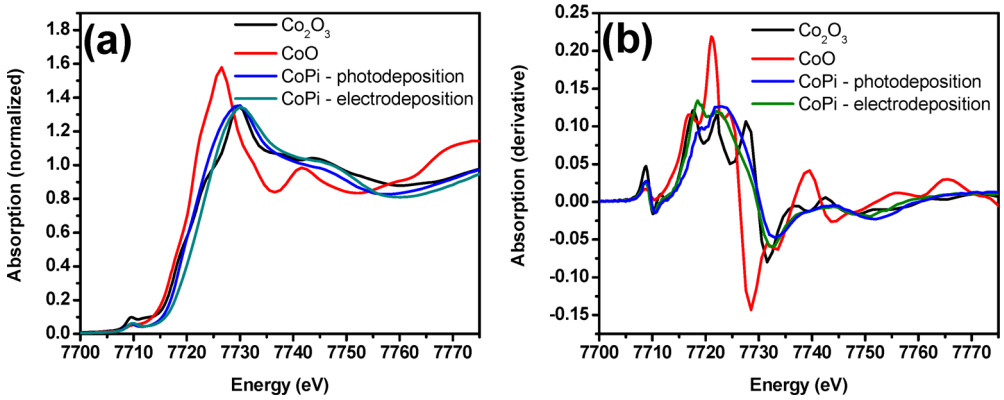

Figure 2. XAFS spectra of the photodeposited and electrodeposited CoPi films on TiO_2, CoO, and Co_2O_3. Black: Co_2O_3; Red: CoO; Blue: photodeposited CoPi; Green: electrodeposited CoPi. (a) XANES spectra of each cobalt sample showing the edge in each instance. (b) First derivative of the energy-space spectra illustrating the energy shift of the CoPi samples relative to CoO.

13-element germanium solid-state detector array, with the fluorescence photon energy window set for the cobalt Kα emission. Upon completion of the deposition, all samples were dried quickly using laboratory tissue (Kimwipe) and then immediately frozen in liquid nitrogen. Samples were then quickly transferred into a cryostat and held at 16 K to prevent any damage to the films over the duration of the experiment. A cobalt foil was placed in between two ionization chambers after the sample and used for the in situ energy calibration. XANES measurements of CoO and Co_2O_3 powders were taken and used as references for the oxidation state of cobalt in the deposited CoPi catalyst. The CoO and Co_2O_3 reference samples were powders diluted in boron nitride by grinding the mixtures. The transmission detection mode was used for the XANES spectra of the references. XAFS data analysis was performed with the Athena and Artemis packages based on IFEFFIT and FEFF programs.[57,58] Theoretical models were constructed in Hyperchem (Hypercube Inc.); the theoretical XAFS spectra were constructed using the FEFF package and were fit to the experimental data using Artemis.[57,58]

RESULTS

Structural Characterization of CoPi on TiO_2. *SEM/EDX.* SEM and EDX experiments were performed on the deposited catalyst following 15 h of photodeposition on the mesoscopic titania electrode films. The SEM images after CoPi photodeposition feature both micrometer and submicrometer size particles of different shapes distributed throughout the semiconductor surface (Figures 1a and b, bright areas), along with a layer of catalyst distributed across the TiO_2 surface as suggested by EDX mapping of both cobalt and phosphate (Supporting Information, Figures S2 and S3). The SEM of the layered catalyst was blurry with some bright spots containing cobalt and phosphate depicted in Figures 1a and b. The EDX elemental analysis indicated the presence of cobalt and phosphate consistent with previously reported CoPi catalysts.[27,36,37] The ratio of Co:P lies between a 1:1 to 2:1 ratio and a strong background from the titania support (Ti) was clearly detected in the EDX profile.

XANES and XAFS Spectra. The XANES spectrum contains information on the structural and electronic characteristics of the X-ray absorbing atom. Figure 2 presents the Co K-edge (7.709 keV) XANES spectra of the CoO and Co_2O_3 model compounds along with the electrodeposited and photodeposited CoPi films on titania. The edge energy of the metal center is defined as the peak of the first derivative of the energy-space spectrum and is related to the oxidation state of the metal center; an increase in net cobalt oxidation state leads to an increase in cobalt edge energy because higher energy X-ray photons are required to eject the 1s electron to the continuum in a metal center with higher positive charges. The cobalt K-edge energy of both CoPi films closely matches that of the Co_2O_3, which indicates that the oxidation state of cobalt in the CoPi films is primarily +3. In addition, all XAFS data presented here were collected on freshly prepared samples in a quasi in situ state at 16 K. These conditions were important to

dx.doi.org/10.1021/cs3005192 | ACS Catal. 2012, 2, 2150−2160

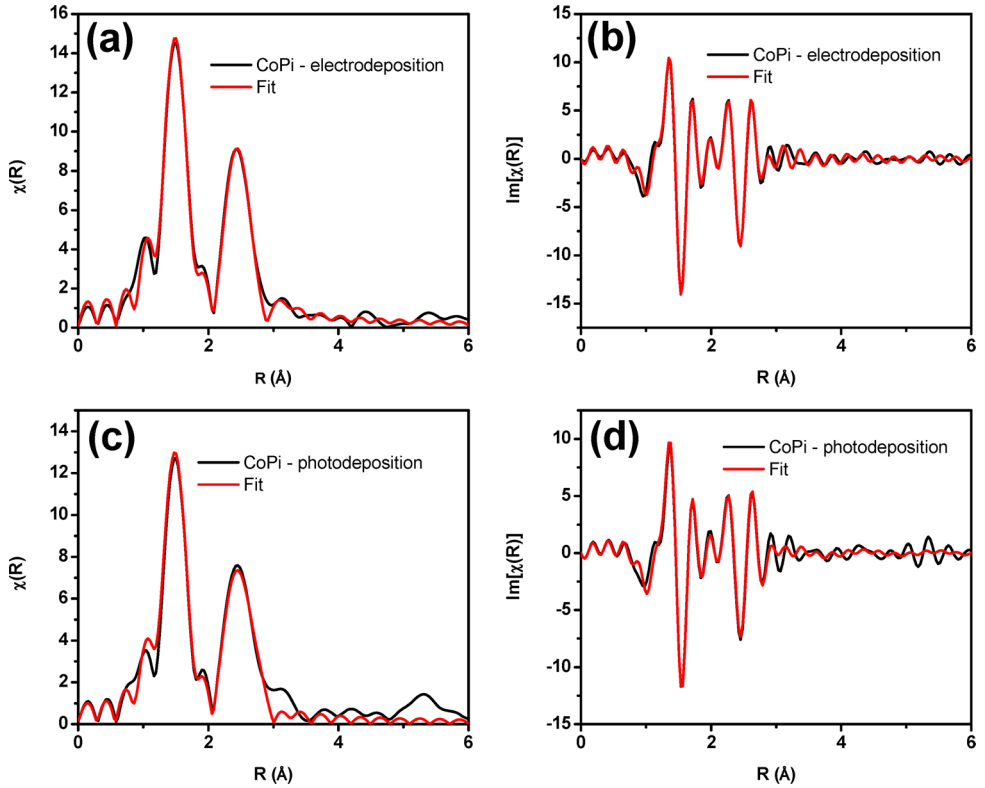

Figure 3. Magnitude and imaginary part of the Fourier transform of electrodeposited and photodeposited CoPi films on titania. Experimental data (black) was fit over an R range of 1.0−2.8 Å (red). Panels (a) and (b) correspond to the magnitude and imaginary portions for the electrodeposited films respectively, while panels (c) and (d) correspond to the magnitude and imaginary portions for the photodeposited films respectively. Fourier transforms were performed over a k-range of 3−13 $Å^{-1}$ using a k-weight of 3.

prevent the catalyst from slowly converting to Co(II) induced by residual water oxidation when subjected to moisture for prolonged time periods under open circuit conditions.[26] In samples where the CoPi OEC were deposited long in advance of the XAFS studies (several days) the primary oxidation state of the cobalt in those samples was +2, consistent with the resting state of the inactivated catalyst.[29,33]

The X-ray absorption fine structure (XAFS) spectrum contains information on the local structure surrounding the X-ray absorbing metal center, for example, cobalt. The postedge oscillations in the XAFS spectrum are caused by the interference between the outgoing photoelectron wave originated from the metal center, such as cobalt, and the back scattered photoelectron waves from the surrounding atoms.[59−61] The Fourier transform of this interference pattern yields a pseudo radial distribution function centered at the Co atoms, where the peaks correspond to specific atom−atom distances. By fitting a theoretical model to the experimental data, the structural parameters corresponding to the structure of the film can be extracted from the following equation.[59−61]

$$\chi(k) = \sum_i F_i(k)\, S_0^2(k) N_i/(kR_0^2)\, \exp(-2\sigma_i^2 k^2)\, \sin[2kR_i + \phi_i(k)]$$

in which $F(k)$ is the magnitude of the backscattering, S_0 the amplitude reduction factor, N the coordination number, R the average distance, σ^2 the mean-squared displacement, and ϕ_i the phase shift; the subscript indicates the ith atom, k the electron wavevector. Figure 3 presents the Fourier-transform of the XAFS of the CoPi films on titania, using a k-range of 3−13 $Å^{-1}$ and a k-weight of 3. Structural models shown in Figure 4 were constructed from Hyperchem (Hypercube Inc.) and used as the

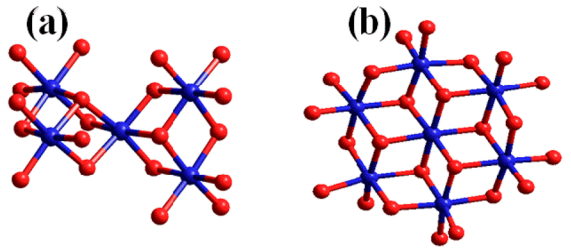

Figure 4. Proposed structures for the CoPi film on titania. (a) Corner-sharing Co-oxo cubane model. (b) Edge-sharing molecular cobaltate cluster (MCC); models were constructed in Hyperchem, and the geometry was optimized using a PM3 semiempirical calculation. The atoms are color coded as cobalt (blue) and oxygen (red).

reference structures in the FEFF calculations to produce reference scattering intensities and pathways. The first model (Figure 4a) with a complete and incomplete CoO cubane structure, and the second model (Figure 4b) with CoO_6 edge-sharing octahedron structure were proposed in previous XAFS experiments and analyses.[32,33,62−64] The structural parameters extracted from the fits for the films from both the electrochemical and photochemical depositions are listed in Tables 1 and 2, respectively. The structures of the films seem to be independent of the deposition technique and consist of 6 μ-oxo oxygen atoms as the nearest neighbors for the cobalt center with a Co−O bond length of ∼1.90 Å. The next coordination

dx.doi.org/10.1021/cs3005192 | ACS Catal. 2012, 2, 2150−2160

Table 1. XAFS Parameters for Electrodeposited CoPi Films on Titania[a]

distance	S_0^2	ΔE	N	R (Å)	σ^2 (Å^{-2})
Co−O	0.70	0.50	6.0	1.90	0.0020
Co−Co	0.70	0.50	3.5	2.81	0.0042

[a] S_0^2, passive reductive factor; ΔE, energy shift; N, coordination number; R, atom−atom distance; σ^2, Debye-Waller factor. The errors for the distances R are about 0.02 Å, and that for the coordination number N is about 0.5.

Table 2. XAFS Parameters for Photodeposition of CoPi Films on Titania[a]

distance	S_0^2	ΔE	N	R (Å)	σ^2 (Å^{-2})
Co−O	0.70	0.33	6.0	1.91	0.0028
Co−Co	0.70	0.33	3.8	2.83	0.0058

[a] All parameters are identical to those in Table 1.

shell contains on average 3.5 and 3.8 Co atoms at an average distance of ∼2.81−2.82 Å.

Electrochemical and Photoelectrochemical Measurements. *TiO_2 Films with Adsorbed Co^{2+}.* All electrochemical measurements as well as oxygen production are done in Co(II)-free solutions of 0.1 M NaPi at pH 7. TiO_2 films were soaked for 15 h in 0.1 M sodium phosphate buffer at pH 7 containing 0.5 mM $Co(NO_3)_2$. CVs (CVs) were recorded at 50 mV/s and revealed a dark quasi-reversible oxidation wave for $Co^{3+/2+}$ at 0.93 V vs Ag/AgCl corresponding to the oxidation of cobalt with hydroxo ligands, immediately followed by a catalytic water oxidation wave (Figure 5a, black).[27,30] The CV under bandgap illumination shows a slight cathodic shift for the onset of the catalytic wave that now overlaps the cobalt oxidation wave. The slight increase of current densities of few μA/cm^2 at low potentials (<0.93 V) with respect to the significant increase in catalytic behavior at >0.93 V lead us to run the controlled potential electrolysis at 1.1 V. Since we were primarily interested in the characterization of the photodeposited catalyst in terms of structure and activity, the deposition time was optimized for the XAFS experiments and electrochemical data, not for photocurrent generation. The dark current (Figure 5b, black) shows a current density of 0.22 mA/cm^2 whereas the photocurrent density (Figure 5b, red) was approximately 0.35 mA/cm^2. Control experiments performed on bare FTO electrodes showed no appreciable current whether the light was on or off at $V_{applied}$ < 1.2 V vs. Ag/AgCl (Figure 5c). The dark current for blank TiO_2 films was almost negligible, and the photocurrent at 1.1 V was only ∼0.04 mA/cm^2 (Figures 5c and 5d).

Short-Circuit Photodeposited CoPi on TiO_2. TiO_2 films decorated with photodeposited CoPi were evaluated for their ability to electrocatalyze water oxidation. The CV of a typical sample reveals the presence of a sharp catalytic wave when recorded in the dark (Figure 6a, black). The photocurrent at low applied potentials (<0.93 V) was <50 μA/cm^2 (Figure 6a,

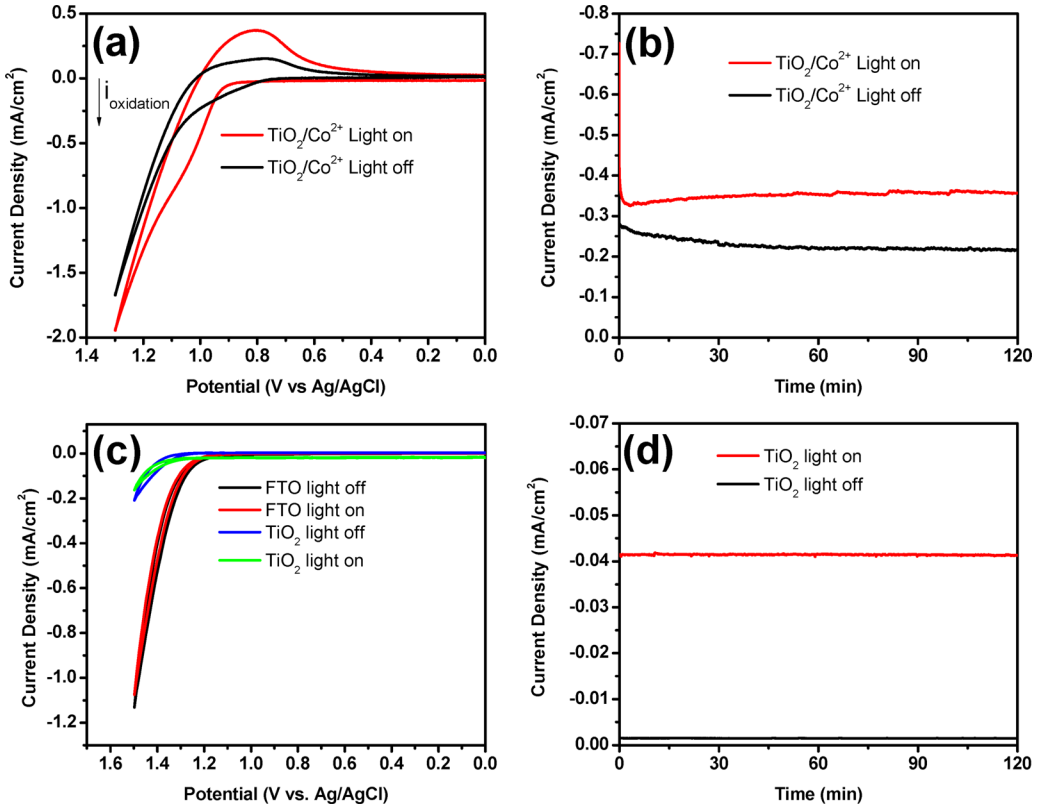

Figure 5. (a) CVs of TiO_2 film electrodes containing Co^{2+} ions adsorbed on the surface recorded at 50 mV/s under broadband illumination (red) and in the dark (black). (b) Controlled potential electrolysis of TiO_2 film electrodes containing Co^{2+} ions adsorbed on the surface at 1.1 V bias under broadband illumination (red) and in the dark (black). (c) CVs performed on FTO glass when the light is off (black line) and on (red line), and TiO_2 films when the broadband light source is off (blue line) and on (green line). The light source was the 200 mW/cm^2 output from a Xe arc lamp passed through a water filter. (d) Controlled potential electrolysis of TiO_2 at 1.1 V bias under broadband illumination (red) and in the dark (black). The electrolyte in all experiments was Co(II)-free solution composed of 0.1 M NaPi buffer at pH 7.

dx.doi.org/10.1021/cs3005192 | ACS Catal. 2012, 2, 2150−2160

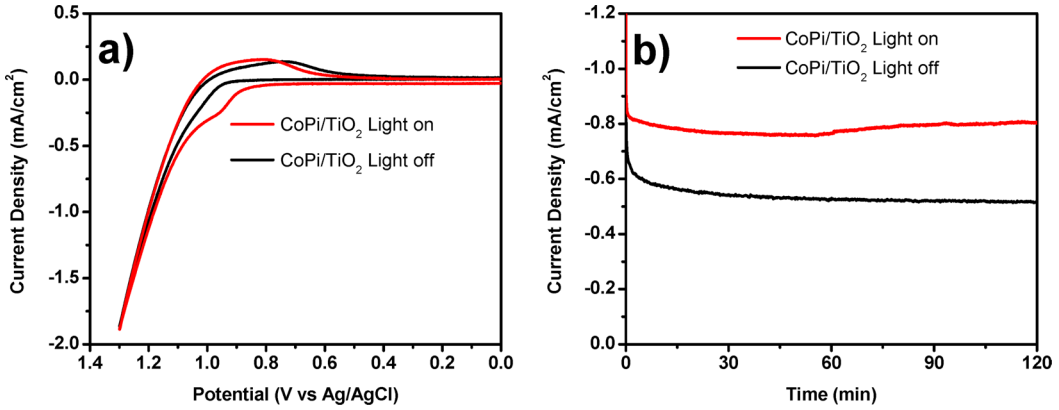

Figure 6. (a) CVs of TiO_2/CoPi subsequent to photodeposition, recorded at 50 mV/s in the presence (red) and absence of broadband illumination (black). (b) Controlled potential electrolysis of TiO_2/CoPi after photodeposition, measured at 1.1 V bias in the presence (red) and absence (black) of broadband illumination. The electrolyte in all experiments was Co(II)-free solution composed of 0.1 M NaPi buffer at pH 7.

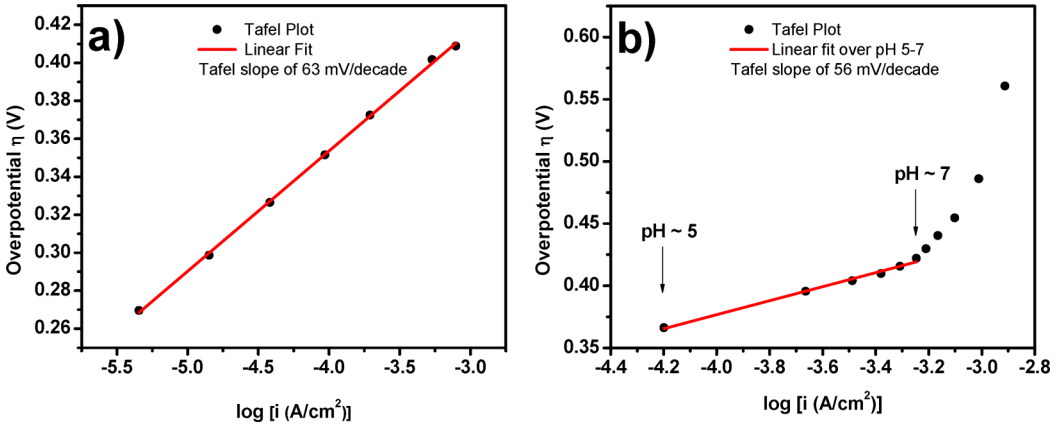

Figure 7. (a) Tafel plot obtained after stepwise increase of the overpotential that was recorded after *iR* correction versus log of the current density. (b) Tafel plot obtained after stepwise increase of pH at 1.1 V vs Ag/AgCl, which was recorded after *iR* correction as overpotential versus log of the current density obtained. In both measurements a fresh TiO_2/CoPi after 15 h photodeposition was used in 0.1 M NaPi buffer at pH 7 containing no Co(II).

red), and the onset of the catalytic wave overlapped the cobalt oxidation (Co^{II}/Co^{III}) peak. The electrolysis performed at 1.1 V generated a dark current density stabilizing at ~0.5 mA/cm^2 after 5 h of continuous electrocatalysis, and a current density of 0.8 mA/cm^2 was produced under broadband illumination at ~200 mW/cm^2 (Figure 6b).

In Figure 7a, the current density in 0.1 M NaPi at pH 7 was recorded as a function of the overpotential for water oxidation, which was calculated based on eq 4.[65]

$$\eta(\mathrm{V}) = V_{\mathrm{appl}} - 0.62 - iR \tag{4}$$

In eq 4, V_{appl} is the applied potential referenced against Ag/AgCl, where E_{anodic} = 0.62 V, the equilibrium potential for water oxidation, i is the current density, and R is the solution resistance as measured by the potentiostat at 0.0 V. In all instances, the current density representative of each data point was permitted to stabilize prior to being recorded. The Tafel plot was measured in the dark using a fresh TiO_2/CoPi electrode and yielded a slope of 63 mV/decade (Figure 7a). In Figure 7b, the current density was measured in 0.1 M NaPi at constant applied potential (1.1 V vs Ag/AgCl) but at varied pH. We assumed Nernstian behavior and corrected for the *iR* drop of the solution to calculate the overpotential in eq 5:

$$\eta(\mathrm{V}) = [V_{\mathrm{appl}} + 0.059 \times \Delta\mathrm{pH} - iR] - 0.62 \tag{5}$$

where most parameters are identical to those in eq 4 and ΔpH = $\mathrm{pH}_{\mathrm{solution}}$ − 7.0, and R is the solution resistance as measured by the potentiostat at 0.0 V at each pH value. The slope obtained from this modified Tafel plot was 56 mV/decade over pH 5−7, and then deviates when the phosphate buffer loses its buffering capacity at pH values higher than its second pK_a (7.2). Operating the electrode under high current densities at pH > pK_{a2} can result in a pH variation across the surface of the electrode as compared to the bulk pH of the solution, which results in a marked decrease of the expected current densities, thereby generating a deviation from the Tafel slope observed between pH 5 to 7 (Figure 7b).

The current density of the photodeposited CoPi film on titania at a 1.1 V applied bias was also measured in a weak proton acceptor electrolyte containing 0.1 M $NaClO_4$ where the current density dropped to ~20 μA/cm^2 in comparison to the NaPi buffer where a 0.5 mA/cm^2 current density was sustained over the long-term, Figure 8.

The oxygen yield was measured by headspace analysis using gas chromatography for the TiO_2/CoPi film in a Co(II)-free NaPi buffer at pH 7 operating in controlled potential electrolysis mode at 1.1 V applied potential, resulting in the sustained generation of oxygen whether the light is off (Figure 9a) or on (Figure 9b). Assuming 100% Faradaic efficiency, the theoretical oxygen yield was calculated by dividing the charge Q

dx.doi.org/10.1021/cs3005192 | ACS Catal. 2012, 2, 2150−2160

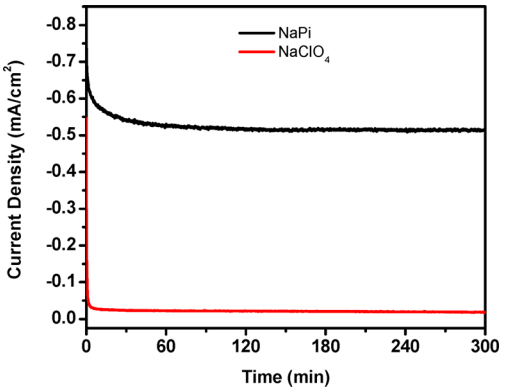

Figure 8. Comparison between the controlled potential electrolysis of CoPi photodeposited on a mesoscopic titania electrode at 1.1 V applied bias in strong proton acceptor 0.1 M NaPi Co(II)-free buffer (black line) and poor proton acceptor 0.1 M $NaClO_4$ Co(II)-free aqueous electrolyte (red line).

(C) passed through the circuit by Faraday's constant, which was subsequently divided by 4 since it takes four hole equivalents to produce one molecule of oxygen. The amount of oxygen measured was corrected for the injection volume and Henry's law. Therefore, the overall Faradaic efficiency is simply the amount of oxygen measured by GC divided by the theoretical yield extracted from the electrochemical charge passed. The product formation analysis presented in Figure 9a indicates that the rate of hydrogen production starts lower than the theoretical one; after 4 h of electrocatalysis the rate become >95% matching the theoretical rate calculated by taking the first derivative of the theoretical number of moles of oxygen versus time (Figure 9a, light off). The initial slow rate of oxygen production detected in the headspace can be attributed to oxygen bubble formation on the electrode surface which does not release in the headspace of the photoelectrochemical cell despite stirring and the excess holes used to maintain the high oxidation state of the catalyst (≥Co(III)). It is worth noting that prolonged photoelectrolysis as well as dark electrolysis performed on the TiO_2/CoPi material produced ~100 ± 5% Faradaic efficiency as ascertained by GC headspace analysis after >10 h of continuous catalysis, during which the amount of oxygen not released in the headspace becomes negligible versus the large amount of oxygen produced. The rate of oxygen production is ~4.5 μmol/h when the light is off, and ~7 μmol/h when the light is on. For illustration purposes, only data from the photoelectrolytic oxygen production measurements are presented in Figure 9b, where the measured amount of oxygen produced and the theoretical yield were plotted when the TiO_2/CoPi electrode was subjected for 17 h to 1.1 V under constant 200 mW/cm^2 irradiation.

DISCUSSION

In previous reports, CoPi has been grown with different macroscopic shapes depending on the length and method of deposition.[27,36,37,39,41,42,44] The ratio of cobalt to phosphate in the catalyst film does not seem to affect the activity of the cobalt-oxo core, especially when one considers that the phosphate ions are most likely terminating the cluster.[33,37] The blurred image in SEM (Figures 1a and 1b) suggests that the catalyst likely renders the surface of titania more insulating and subsequently prone to charging effects from the electron beam.[39] In this study, we were interested in the characterization of the as-deposited catalytic material. Hence, the deposition time was more elongated than previously reported materials,[36−39] where the magnitude of deposition was assessed based on photocurrent optimization. In this regard, it is important to note that the dark brown CoPi catalyst deposited on TiO_2 (Supporting Information, Figure S1) will eventually have large competitive absorption for bandgap photons. To alleviate this effect, the photodeposition was performed using front-side illumination of the films, and the photocurrent measurements were accomplished using backside illumination of these films.

The first model structure (Figure 4a) used in the XAFS fitting of the electrochemically and photochemically deposited films was a simple CoO cubane structure, similar to that previously proposed.[32] Both the Co−O and Co−Co bond distances (1.89 Å and 2.81 Å, respectively) fit those in the model. The average Co-Co distance of 2.81 Å is consistent with two Co atoms connected by a μ-oxo bridge.[32] The average first and second shell coordination numbers from this model are 6.0 and 2.4, respectively. While the coordination number for the cobalt with the first shell oxygen atoms agrees with the experimental value, the coordination number for the second

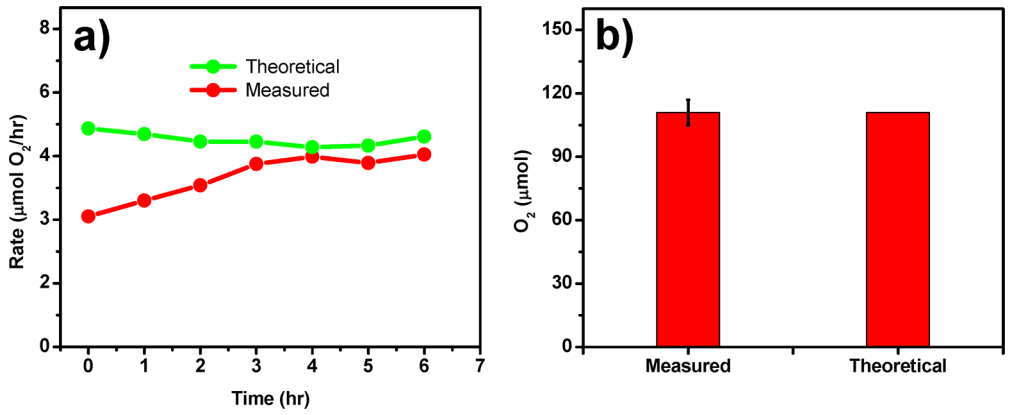

Figure 9. (a) Theoretical rate of O_2 produced in the dark calculated from the current/time plot produced under controlled potential electrolysis of a photodeposited CoPi film on a mesoscopic titania electrode under 1.1 V applied bias (black) and the corresponding rate of O_2 evolved as measured by GC headspace analysis produced in the identical sample (red). (b) Oxygen evolution as measured by GC headspace analysis compared with the theoretical yield after 17 h photoelectrolysis of the same sample at 1.1 V applied bias under 200 mW/cm^2 backside illumination. The electrolyte in all experiments was Co(II)-free solution composed of 0.1 M NaPi buffer at pH 7.

dx.doi.org/10.1021/cs3005192 | ACS Catal. 2012, 2, 2150−2160

coordination shell (Co−Co) from fitting the experimental data were 3.5 and 3.8 for the electrochemically and photochemically deposited films, respectively. According to the structure in Figure 4a, one central Co atom has a coordination number of 4 for the second coordination shell Co−Co distances, while each of the four peripheral Co atoms has a coordination number of 2 corresponding to the same Co−Co coordinating shell. Hence the average coordination number for the Co−Co shell in this cluster model should be $(4 + 4 \times 2)/5 = 2.4$, which is much lower than the values of 3.5 or 3.8 obtained from the fitting. Using the model structure in Figure 4b, the Co−Co coordination numbers for the central Co atom is 6 and for each of the six peripheral Co atoms is 3. The average coordination number for the Co−Co shell in the structure shown in Figure 4b is therefore $(6 + 6 \times 3)/7 = 3.43$, which is much closer to the experimental values listed in Tables 1 and 2. Hence, the XAFS results for the catalysts prepared electrochemically and photochemically on titania prefer an edge-sharing molecular cobaltate cluster (MCC) similar to the structural model suggested by Nocera and co-workers, Figure 4b.[33] In addition, X-ray pair distribution function (PDF) analysis and high-energy X-ray scattering experiments performed at room temperature in the atmosphere on the electrodeposited "CoPi" catalyst suggested multiple edge-sharing CoO_6 octahedra consisting of total 13−14 cobalt atoms with possible distorted geometries at the domain edges.[66] However, their conditions for sample measurements (i.e., at room temperature in the atmosphere) differ from ours (i.e., cooled immediately in liquid nitrogen after being prepared and then measured at 16 K in vacuum). It is important to note from our results that the electrochemically deposited film and the photochemically deposited film on titania are indistinguishable within the resolution of the XAFS experiment, indicating that equivalent films are likely generated regardless of deposition technique. Originally, the MCC model was proposed based on a prepared "bulk" CoPi analyzed in situ, since this type of structure can support Co−Co coordination numbers >4.[33] Our XAFS results are also in favor of the edge-sharing CoO_6 octahedra for both the electrodeposited and photodeposited CoPi on mesoscopic titania, confirming the in situ XAFS data and other electrochemical experiments performed on similar materials.[30,33,64]

The presence of photodeposited CoPi enhanced the photocurrents at high potentials (>0.93 V) as compared with the "naked" TiO_2 or TiO_2 bearing adsorbed Co(II) which indicates the formation of additional catalytic sites for water oxidation in the former, and a possible decrease of charge recombination sites, which are primary prerequisites for photocurrent enhancement.[37,53] The dark current density arising from this photodeposited catalyst was promising given the low coverage of cobalt on TiO_2 as compared with electrodeposited films of several micrometer thickness on conductive glass which gave ∼1 mA/cm^2 at 1.1 V vs Ag/AgCl.[27] In addition, the photochemically grown catalyst was shown to be electrochemically active toward water oxidation. These results complement previous reports which demonstrated that electrochemically formed CoPi on $BiVO_4$ acted as an efficient photocatalyst for oxygen production.[43]

The increase of one pH unit in the window of operating pH was equivalent to increasing the overpotential by ∼59 mV, Figure 7. The Tafel slope of 59 mV/decade, which is equivalent to $2.3RT/F$ (Figure 7) and the strong proton acceptor electrolyte requirement (Figure 8) suggest a proton-coupled electron transfer (PCET) process prior to the rate limiting oxygen evolution step.[12,28,30,31,65,67,68] The drastic drop of current density in $NaClO_4$ electrolyte versus the sustainably of catalysis in NaPi buffer (Figure 8) demonstrates the necessity of phosphate to act as proton acceptor in the oxygen evolution cycle. In fact, proton transfer is considered a very important step in the oxygen production mechanism of CoPi, and $NaClO_4$ is a weak proton acceptor, rendering oxygen evolution inoperable. A rapid one-electron coupled to one-proton equilibrium between Co^{III}−OH and Co^{IV}−O most likely occurs before the oxygen production step, with the involvement of bridging oxygen atoms, analogous to the electrodeposited CoPi catalyst.[11,29,30] This PCET was suggested to be a core step of the mechanism of oxygen evolution, and the subsequent self-healing property upon reapplication of potential following catalyst dissolution; the latter could be induced by simply subjecting the electrodeposited CoPi to open-circuit conditions.[26,29,31] During prolonged controlled potential photoelectrolysis measurements performed for 17 h at 1.1 V applied bias, the TiO_2/CoPi system yielded ∼100 ± 5% current to oxygen conversion efficiencies (Figure 9b). This efficiency was the same whether the light is on or off, indicating that the holes supplied to the catalyst via electrochemical and photochemical methods are equivalent in terms of oxygen product formation once the CoPi catalyst is formed on the surface of TiO_2. All these combined results confirm that the photochemically grown catalyst is similar in terms of activity to the electrochemically formed films, with both operating with near unity Faradaic efficiencies for oxygen production.

CONCLUSIONS

The CoPi OEC was photodeposited on mesoscopic TiO_2 films whose structure and electrocatalytic activity was characterized using a variety of techniques and illustrated remarkable consistency with the analogous established electrodeposited materials, already shown to be superior catalysts enabling water oxidation at neutral pH. The structure of the photodeposited CoPi material on titania is most likely composed of molecular cobaltate clusters featuring edge-sharing CoO_6 octahedra wherein water oxidation occurs through a series of redox processes involving proton coupled electron transfer prior to the ultimate oxygen evolving event. The OEC catalyst operated at near unity Faradaic efficiencies in controlled potential electrolysis experiments, indicating that the holes relayed to the photodeposited CoPi are indeed selective for promoting water oxidation on mesoscopic titania electrodes. The quantitative similarity in structure and operational mechanism of the water oxidation process strongly suggests that materials formed as a result of in situ photodeposition on wide bandgap metal oxides represent a viable strategy for the synthesis of next generation catalysts using earth abundant elements.

ASSOCIATED CONTENT

Supporting Information

Photographs of TiO_2 and TiO_2/CoPi films, EDX mapping of cobalt and phosphate on TiO_2 after 15-h CoPi photodeposition, XAFS and EDX evidence of Co(II) and phosphate adsorption on TiO_2, and SEM/EDX of CoPi electrodeposited on the mesoscopic TiO_2 substrate. This material is available free of charge via the Internet at http://pubs.acs.org.

AUTHOR INFORMATION

Corresponding Author

*E-mail: castell@bgsu.edu (F.N.C.), lchen@anl.gov (L.X.C.).

Funding

The BGSU portion of the work was supported by the National Science Foundation (CHE-1012487). A part of research at Argonne National Laboratory in the Chemical Sciences and Engineering Division was supported by the U.S. Department of Energy, Office of Science, Office of Basic Energy Sciences, under Contract DE-AC02-06CH11357. Work at the Argonne National Laboratory Advanced Photon Source was supported by the U.S. Department of Energy, Office of Science, Office of Basic Energy Sciences, under Contract DE-AC02-06CH11357.

Notes

The authors declare no competing financial interest.

ACKNOWLEDGMENTS

We would like to thank Dr. Marilyn Cayer for her assistance with the SEM/EDX measurements and Argonne National Laboratory for allocating the experimental facilities used to acquire XAFS and XANES spectra.

REFERENCES

(1) Esswein, A. J.; Nocera, D. G. *Chem. Rev.* **2007**, *107*, 4022−4047.
(2) Norris Jr., J. R., Meisel, D., Eds.; *Photochemical Energy Conversion*; Elsevier: New York, 1989.
(3) Gratzel, M., Ed.; *Energy resources through photochemistry and catalysis*; Academic Press: New York, 1983.
(4) Heyduk, A. F.; Nocera, D. G. *Science* **2001**, *293*, 1639−1641.
(5) Gray, H. B.; Maverick, A. W. *Science* **1981**, *214*, 1201−1205.
(6) Lewis, N. S.; Nocera, D. G. *Proc. Natl. Acad. Sci. U.S.A.* **2006**, *103*, 15729−15735.
(7) Jacobson, M. Z. *Energy Environ. Sci.* **2009**, *2*, 148−173.
(8) Holtz-Eakin, D.; Selden, T. M. *J. Public Econ.* **1992**, *57*, 85−101.
(9) Gratzel, M. *Nature* **2001**, *414*, 338−344.
(10) Wrighton, M. S. *Acc. Chem. Res.* **1979**, *12*, 303−310.
(11) Nocera, D. G. *Acc. Chem. Res.* **2012**, *45*, 767−776.
(12) Reece, S. Y.; Hamel, J. A.; Sung, K.; Jarvi, T. D.; Esswein, A. J.; Pijpers, J. J. H.; Nocera, D. G. *Science* **2011**, *334*, 645−648.
(13) Nocera, D. G. *Energy Environ. Sci.* **2010**, *3*, 993−995.
(14) Nocera, D. G. *ChemSusChem* **2009**, *2*, 387−390.
(15) Shevchenko, D.; Anderlund, M. F.; Thapper, A.; Styring, S. *Energy Environ. Sci.* **2011**, *4*, 1284−1287.
(16) Dinca, M.; Surendranath, Y.; Nocera, D. G. *Proc. Natl. Acad. Sci. U.S.A.* **2010**, *107*, 10337−10341.
(17) Kanan, M. W.; Surendranath, Y.; Nocera, D. G. *Chem. Soc. Rev.* **2009**, *38*, 109−114.
(18) Youngblood, W. J.; Lee, S. H. A.; Kobayashi, Y.; Hernandez-Pagan, E. A.; Hoertz, P. G.; Moore, T. A.; Moore, A. L.; Gust, D.; Mallouk, T. E. *J. Am. Chem. Soc.* **2009**, *131*, 926−927.
(19) Yin, Q.; Tan, J. M.; Besson, C.; Geletii, Y. V.; Musaev, D. G.; Kuznetsov, A. E.; Luo, Z.; Hardcastle, K. I.; Hill, C. L. *Science* **2010**, *328*, 342−345.
(20) Concepcion, J. J.; Jurss, J. W.; Brennaman, M. K.; Hoertz, P. G.; Patrocinio, A. O. v. T.; Murakami Iha, N. Y.; Templeton, J. L.; Meyer, T. J. *Acc. Chem. Res.* **2009**, *42*, 1954−1965.
(21) Huynh, M. H. V.; Meyer, T. J. *Chem. Rev.* **2007**, *107*, 5004−5064.
(22) Dempsey, J. L.; Esswein, A. J.; Manke, D. R.; Rosenthal, J.; Soper, J. D.; Nocera, D. G. *Inorg. Chem.* **2005**, *44*, 6879−6892.
(23) Shafirovich, V. Y.; Khannanov, N. K.; Strelets, V. V. *Nouv. J. Chim.* **1980**, *4*, 81−84.
(24) Shafirovich, V. Y.; Strelets, V. V. *Nouv. J. Chim.* **1978**, *2*, 199−201.
(25) Esswein, A. J.; Surendranath, Y.; Reece, S. Y.; Nocera, D. G. *Energy Environ. Sci.* **2011**, *4*, 499−504.
(26) Lutterman, D. A.; Surendranath, Y.; Nocera, D. G. *J. Am. Chem. Soc.* **2009**, *131*, 3838−3839.
(27) Kanan, M. W.; Nocera, D. G. *Science* **2008**, *321*, 1072−1075.
(28) Symes, M. D.; Surendranath, Y.; Lutterman, D. A.; Nocera, D. G. *J. Am. Chem. Soc.* **2011**, *133*, 5174−5177.
(29) Surendranath, Y.; Kanan, M. W.; Nocera, D. G. *J. Am. Chem. Soc.* **2010**, *132*, 16501−16509.
(30) Gerken, J. B.; McAlpin, J. G.; Chen, J. Y. C.; Rigsby, M. L.; Casey, W. H.; Britt, R. D.; Stahl, S. S. *J. Am. Chem. Soc.* **2011**, *133*, 14431−14442.
(31) Surendranath, Y.; Dinca, M.; Nocera, D. G. *J. Am. Chem. Soc.* **2009**, *131*, 2615−2620.
(32) Risch, M.; Khare, V.; Zaharieva, I.; Gerencser, L.; Chernev, P.; Dau, H. *J. Am. Chem. Soc.* **2009**, *131*, 6936−6937.
(33) Kanan, M. W.; Yano, J.; Surendranath, Y.; Dincă, M.; Yachandra, V. K.; Nocera, D. G. *J. Am. Chem. Soc.* **2010**, *132*, 13692−13701.
(34) McAlpin, J. G.; Surendranath, Y.; Dinca, M.; Stich, T. A.; Stoian, S. A.; Casey, W. H.; Nocera, D. G.; Britt, R. D. *J. Am. Chem. Soc.* **2010**, *132*, 6882−6883.
(35) McDonald, K. J.; Choi, K.-S. *Chem. Mater.* **2011**, *23*, 4863−4869.
(36) McDonald, K. J.; Choi, K.-S. *Chem. Mater.* **2011**, *23*, 1686−1693.
(37) Steinmiller, E. M. P.; Choi, K. S. *Proc. Natl. Acad. Sci. U.S.A.* **2009**, *106*, 20633−20636.
(38) Hong, Y.-R.; Liu, Z.; Al-Bukhari, S. F. B. S. A.; Lee, C. J. J.; Yung, D. L.; Chi, D.; Hor, T. S. A. *Chem. Commun.* **2011**, *47*, 10653−10655.
(39) Zhong, D. K.; Cornuz, M.; Sivula, K.; Graetzel, M.; Gamelin, D. R. *Energy Environ. Sci.* **2011**, *4*, 1759−1764.
(40) Zhong, D. K.; Sun, J.; Inumaru, H.; Gamelin, D. R. *J. Am. Chem. Soc.* **2009**, *131*, 6086−6087.
(41) Zhong, D. K.; Gamelin, D. R. *J. Am. Chem. Soc.* **2010**, *132*, 4202−4207.
(42) Seabold, J. A.; Choi, K.-S. *Chem. Mater.* **2011**, *23*, 1105−1112.
(43) Wang, D.; Li, R.; Zhu, J.; Shi, J.; Han, J.; Zong, X.; Li, C. *J. Phys. Chem. C* **2012**, *116*, 5082−5089.
(44) Zhong, D. K.; Choi, S.; Gamelin, D. R. *J. Am. Chem. Soc.* **2011**, *133*, 18370−18377.
(45) Pilli, S. K.; Furtak, T. E.; Brown, L. D.; Deutsch, T. G.; Turner, J. A.; Herring, A. M. *Energy Environ. Sci.* **2011**, *4*, 5028−5034.
(46) Higashi, M.; Domen, K.; Abe, R. *J. Am. Chem. Soc.* **2012**, *134*, 6968−6971.
(47) Young, E. R.; Costi, R.; Paydavosi, S.; Nocera, D. G.; Bulovic, V. *Energy Environ. Sci.* **2011**, *4*, 2058−2061.
(48) Pijpers, J. J. H.; Winkler, M. T.; Surendranath, Y.; Buonassisi, T.; Nocera, D. G. *Proc. Natl. Acad. Sci. U.S.A.* **2011**, *108*, 10056−10061.
(49) Leung, D. Y. C.; Fu, X. L.; Wang, C. F.; Ni, M.; Leung, M. K. H.; Wang, X. X.; Fu, X. Z. *ChemSusChem* **2010**, *3*, 681−694.
(50) Fujishima, A.; Kohayakawa, K.; Honda, K. *J. Electrochem. Soc.* **1975**, *122*, 1487−1489.
(51) Fujishima, A.; Zhang, X. T.; Tryk, D. A. *Surf. Sci. Rep.* **2008**, *63*, 515−582.
(52) Fujishima, A.; Honda, K. *Nature* **1972**, *238*, 37−38.
(53) Hoang, S.; Guo, S.; Hahn, N. T.; Bard, A. J.; Mullins, C. B. *Nano Lett.* **2012**, *12*, 26−32.
(54) Kay, A.; Cesar, I.; Grätzel, M. *J. Am. Chem. Soc.* **2006**, *128*, 15714−15721.
(55) Lee, S.-H. A.; Abrams, N. M.; Hoertz, P. G.; Barber, G. D.; Halaoui, L. I.; Mallouk, T. E. *J. Phys. Chem. B* **2008**, *112*, 14415−14421.
(56) Onicha, A. C.; Castellano, F. N. *J. Phys. Chem. C* **2010**, *114*, 6831−6840.
(57) Newville, M. *J. Synchrotron Rad.* **2001**, *8*, 322−324.
(58) Ravel, B.; Newville, M. *J. Synchrotron Rad.* **2005**, *12*, 537−541.
(59) Lytle, F. W.; Sayers, D. E.; Stern, E. A. *Phys. Rev. B* **1975**, *11*, 4825−4835.
(60) Stern, E. A.; Sayers, D. E.; Lytle, F. W. *Phys. Rev. B* **1975**, *11*, 4836−4846.

(61) Sayers, D. E.; Stern, E. A.; Lytle, F. *Phys. Rev. Lett.* **1971**, *27*, 1204−1207.
(62) Mattioli, G.; Risch, M.; Bonapasta, A. A.; Dau, H.; Guidoni, L. *Phys. Chem. Chem. Phys.* **2011**, *13*, 15437−15441.
(63) Pecoraro, V.; Brudvig, G.; Dau, H.; Aukauloo, A.; Nocera, D.; Siegbalm, P.; Messinger, J. *Phil. Trans. R. Soc. B* **2008**, *363*, 1218−1219.
(64) Risch, M.; Klingan, K.; Ringleb, F.; Chernev, P.; Zaharieva, I.; Fischer, A.; Dau, H. *ChemSusChem* **2012**, *5*, 542−549.
(65) Gileadi, E. *Electrode Kinetics for Chemists, Chemical Engineers, and Materials Scientists*; Wiley-VCH: New York, 1993.
(66) Du, P.; Kokhan, O.; Chapman, K. W.; Chupas, P. J.; Tiede, D. M. *J. Am. Chem. Soc.* **2012**, *134*, 11096−11099.
(67) McAlpin, J. G.; Stich, T. A.; Ohlin, C. A.; Surendranath, Y.; Nocera, D. G.; Casey, W. H.; Britt, R. D. *J. Am. Chem. Soc.* **2011**, *133*, 15444−15452.
(68) Surendranath, Y.; Lutterman, D. A.; Liu, Y.; Nocera, D. G. *J. Am. Chem. Soc.* **2012**, *134*, 6326−6336.